

Isotherm and kinetic studies on adsorption of malachite green using chemically synthesized silver nanoparticles

A. Muthu Kumara Pandian¹ · C. Karthikeyan¹ · M. Rajasimman¹

Received: 25 July 2016 / Accepted: 28 November 2016 / Published online: 2 January 2017
© Springer International Publishing Switzerland 2016

Abstract In the present study, chemically synthesized silver nanoparticles (AgNPs) were used for adsorption of the dye malachite green (MG). The process variables such as nanoparticle dosage, pH and temperature were optimized for the decolourization of MG dye solution using the response surface methodology (RSM). At the optimized parameter condition, studies were carried out for effects with respect to various concentrations of dye and time for isotherm and kinetic studies, respectively. RSM was also employed for the enhanced production of silver nanoparticles (AgNPs). Synthesized AgNPs were characterized by UV–Vis spectroscopic, scanning electron microscopic and Fourier transform infrared analyses. From the results, it was concluded that the AgNPs readily decolourized MG dye. At the optimized conditions, maximum removal (more than 90%) of MG dye occurred. It was also found that the D–R isotherm and intraparticle diffusion fitted the data better as compared to other isotherm and kinetic models.

Keywords Nanoparticle · Adsorption · MG · Silver · RSM · Optimization

Introduction

AgNPs can be synthesized by different methods. Broadly, they can be categorized as chemical and biological methods. Biological methods comprise both the plants and microorganisms. The main advantages of chemical method for the synthesis of nanoparticles over the biological are less time consumption and easier production [34]. Dyes have major applications in industries, viz. paper and pulp, textiles, adhesives, art supplies, beverages, ceramics, construction, cosmetics, food, glass, paints, polymer, soap, wax biomedicine. Various dyes are manufactured to meet the requirement of each type of industries. Thus, with this whole range of use, its impact on the environment is also wide. They cause various hazards and health-related effects [5]. The families of chemical compounds that make good dyes are toxic to humans. One such dye is malachite green.

MG is traditionally used as dye. Huge quantity of MG and related triarylmethane dyes are produced annually for this purpose [15]. Animals metabolize malachite green in its leuco form, and they are retained in catfish muscle longer than its parent molecule [70–72]. There is also possibility that MG caused carcinogenic symptoms [9]. However, its use is inevitable due to wide range of applications. Thus, it is necessary to treat the dye-containing waste water before they are discharged into the environment in order to reduce its harmful effects.

There are few works available on the removal of dyes by AgNPs [25, 62] synthesized by biological methods. So far, no work has been carried out for the enhancement of AgNPs production. Hence, the objectives of the present study are to enhance the production of AgNPs by chemical method using RSM and to check the efficiency of synthesized AgNPs for the removal of MG dye.

✉ A. Muthu Kumara Pandian
mkp.asokan@gmail.com

¹ Environmental Engineering Laboratory, Department of Chemical Engineering, Annamalai University, Annamalai Nagar, Chidambaram, Tamil Nadu 608002, India

Materials and methods

Chemicals

All chemicals used in this study were of analytical grade. Silver nitrate and trisodium citrate were purchased from Himedia Labs, India. The silver nitrate was stored in dark-coloured bottles. Solution of silver nitrate was prepared using deionized water. The solution was stored in refrigerator in a dark-coloured bottle for future use. It avoids photosensitive reaction of silver nitrate when exposed to light. Synthetic malachite green was purchased from Merck Ltd., India.

Experimental design by RSM

RSM is a statistical tool designed to find out the optimal response within specific ranges of pre-established factors, through second-order equation. In this work, central composite design (CCD) and Box–Behnken design (BBD) were used to study the effects of parameters during synthesis and decolourization process, respectively. The coded values of the process parameters were determined by the following equation:

$$X_i = \frac{X_i - X_o}{\Delta X} \quad (1)$$

where X_i is coded value of the i th variable, X_i uncoded value of the i th test variable, and X_o uncoded value of the i th test variable at centre point. The regression analysis was performed to estimate the response function as a second-order polynomial.

A second-order polynomial equation is:

$$Y = \beta_0 + \sum_{i=1}^k \beta_i X_i + \sum_{i=1}^k \beta_{ii} X_i^2 + \sum_{i=1, i > j}^{k-1} \sum_j^k \beta_{ij} X_i X_j \quad (2)$$

where Y is the predicted response and β_i , β_j , β_{ij} are coefficients estimated from regression and represent the linear, quadratic and cross-products of X_1 , X_2 , X_3 on response.

A statistical program package Design Expert 7.1.5 was used for regression analysis of the data obtained and to estimate the coefficient of the regression equation. The equation was validated by ANOVA. All the experiments were performed in triplicate, and average value was reported.

CCD for maximum production of AgNPs

In order to perform the dye decolourization experiment, large quantities of AgNPs are required to carry out series of runs. Thus, there is a need for maximum production of AgNPs. Hence, response surface methodology was used to

Table 1 Experimental range and levels of independent process variables for AgNPs production

Independent variable	Coded levels					
	Code	-1.68	-1	0	+1	+1.68
pH	A	4.9	5.5	7	8.5	9.1
Conc. of AgNO ₃ (mg/mL)	B	0.6	1	2	3	3.4

find the optimum conditions for maximum production of AgNPs. The parameters, viz. silver nitrate concentration and pH, were optimized to yield maximum quantity of AgNPs. The ranges of pH and silver nitrate concentration are given in Table 1.

Procedure for chemical synthesis of AgNPs

Fifty millilitres of 10^{-3} M silver nitrate solution was heated to boiling. To this solution, 5 mL of 1% trisodium citrate was added drop by drop. During this process, solution was mixed vigorously and heated until the colour change was evident (dark brown). Then, it was removed from the heating element and stirred until it reaches room temperature. The aqueous solution was lyophilized, and the powdered AgNPs obtained were taken for further analysis [45].

Characterization of AgNPs

UV–visible spectroscopy analysis

Synthesis of AgNPs is visually confirmed by the transformation of the pale white-coloured silver nitrate solution into dark brown-coloured solution. Primarily, the formation of AgNPs was confirmed by the absorption spectra of the synthesized AgNPs solution. The synthesized silver nanoparticles were scanned in the range 200–800 nm.

Fourier transform infrared spectroscopy

FTIR studies were carried for both fresh and MG-loaded AgNPs. It gives information about the respective functional groups present in the AgNPs before and after the adsorption process.

Scanning electron microscopy

It is important to study the morphology of the AgNPs. The morphology of the AgNPs changes after the treatment. Thus, SEM images of the AgNPs before and after treatments were taken.

Table 2 Experimental range and levels of independent process variables for decolourization of MG using synthesized AgNPs

Independent variable	Coded levels			
	Code	-1	0	1
pH	A	5	7	9
Temperature (°C)	B	30	45	60
AgNPs dosage (g)	C	0.1	0.5	0.9

Batch adsorption experiment for malachite green

The batch experiments for the removal of MG dye were carried out according to the BBD. The range and levels of the individual variables are shown in Table 2. Initial concentration of the dye was fixed as 100 ppm. The experiments were carried out in a 250-mL conical flask. The reaction mixtures were agitated in incubated shaker, and samples were centrifuged at 10,000 rpm for 15 min. The supernatant was used for the analysis of dye concentration using spectrophotometer. The analyses were repeated three times so as to analyse the results statistically. The amount of dye adsorbed per unit mass of adsorbent (q_e , mg/g) is given by Eq. (3):

$$q_e = \frac{(C_o - C_e)V}{m} \tag{3}$$

The amount of adsorbed dye per unit mass of adsorbent at time t (q_t , mg/g) is:

$$q_t = \frac{(C_o - C_t)V}{m} \tag{4}$$

where V is the volume of the solution treated in L, C_o is the initial concentration of the dye in mg/L, C_e is the

equilibrium dye concentration in mg/L, C_t (mg/L) is the concentration of adsorbent at time t , and m is the mass of adsorbent in gram. At the optimized conditions of pH, temperature and sorbent dosage, experiments were performed.

Results and discussion

AgNPs production maximization study

The maximization of the AgNPs production was carried out according to the CCD, and the results obtained are given in Table 3. The results of theoretically predicted response are also given in Table 3. The mathematical expression of relationship to the response with variables is:

$$Y = 1.80 + 0.050A + 0.24B + 0.040AB - 0.56A^2 - 0.64B^2 \tag{5}$$

where Y is the quantity of AgNO₃(g) and A and B are the coded values of pH and concentration of AgNO₃, respectively.

The ANOVA results for AgNPs production are tabulated in Table 4. F value of 24.98 implies that the model was significant. The Fisher F test with a very low probability value ($P_{model} > 0.0001$) reveals a very high significance for the regression model. The goodness of fit of the model was checked by coefficient of determination (R^2). The R^2 was found to be 0.9469, which implies that more than 94.69% of experimental data were compatible with the data predicted by the model. A low coefficient of variation (CV) value (18.83) indicates that the deviations between experimental and predicted values were low. Adeq precision

Table 3 CCD and its response for AgNPs production

Run order	A (pH)	B (conc. of AgNO ₃) (g/L)	Quantity of AgNPs (g)	
			Experimental	Predicted
1	0 (7)	0 (2)	1.80	1.903
2	0 (7)	-2 (0.6)	0.30	0.289
3	-2 (4.9)	0 (2)	0.80	0.702
4	0 (7)	0 (2)	0.80	1.903
5	2 (9.1)	0 (2)	0.90	0.844
6	0 (7)	0 (2)	1.80	0.957
7	0 (7)	2 (3.4)	1.10	0.266
8	1 (8.5)	-1 (1)	0.25	0.638
9	-1 (5.5)	1 (3)	0.50	1.697
10	0 (7)	0 (2)	1.80	0.819
11	1 (8.5)	1 (3)	0.71	0.246
12	-1 (5.5)	-1 (1)	0.20	1.697
13	0 (7)	0 (2)	1.80	1.697
14	0 (7)	0 (2)	1.80	1.697

Table 4 ANOVA for production maximization of AgNPs

Source	Sum of squares	df	Mean square	F value	P value
Model	4.96	5	0.99	24.98	0.0003
A	0.020	1	0.020	0.51	0.4995
B	0.45	1	0.45	11.25	0.0122
AB	6.400	1	6.400	0.16	0.7002
A ²	2.22	1	2.22	55.88	0.0001
B ²	2.85	1	2.85	71.70	<0.0001
Residual	0.28	7	0.040		
Lack of fit	0.28	3	0.093		
Pure error	0.000	4	0.000		
Cor total	5.24	12			

SD 0.20, R² 0.9469, mean 1.06, adj. R² 0.9090, CV% 18.83, pred. R² 0.6226, PRESS 1.98, Adeq precision 11.920

measures the signal-to-noise ratio. A ratio >4 is desirable. In this study, the ratio was found to be 11.920, which indicates an adequate signal. Values of “P” < 0.05 indicate the significance of model terms. In this case, B, A² and B² were significant model terms for the maximum production of AgNPs. This implies that the linear and square effects of pH and concentration of AgNO₃ were significant factors.

Effect of variables on AgNPs production

The formation of AgNPs depends on various parameters such as pH and concentration of AgNO₃.

Effect of pH and concentration of AgNO₃ on production of AgNPs

The effect of pH on the production of AgNPs was studied by changing the pH from 4.9 to 9.1. The results obtained are shown in Fig. 1. It was observed from the plot that near-neutral pH range of 6.5–7.5 enhanced AgNPs production observed and maximum production of AgNPs was obtained at pH 7.2. Further increase or decrease in pH decreased production of AgNPs. The effect of concentration of AgNO₃ on the production of AgNPs was studied by changing the concentration from 0.6 to 3.4 mg/mL. The result obtained is shown in Fig. 1. It was observed from the plot that enhanced AgNPs production was obtained around concentration range of 1.5–2.5 mg/mL and maximum production of AgNPs was observed at 2.2 mg/mL. Further increase or decrease in concentration of AgNO₃ decreases production of AgNPs. Temperature is also an important variable for the production of AgNPs, but in this method of synthesis of AgNPs, the solution mixture should be boiled in order to produce the AgNPs. Therefore, it is kept as constant. Figure 2 shows the perturbation plot for AgNP production. In the plot, both A and B curves are more

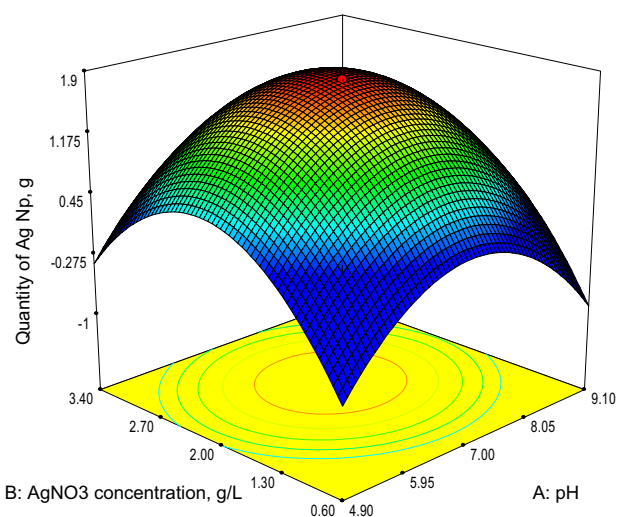


Fig. 1 Interactive effect of pH and concentration of AgNO₃ on AgNPs production

similar in curvature. It shows significant effect of both pH and AgNO₃ concentration.

UV-visible spectroscopy analysis

The physical confirmation of AgNPs formation was by the colour change of pale white silver nitrate solution to dark brown. It is due to the surface plasmon resonance [43]. From Fig. 3, it was observed that the characteristic AgNPs peak was obtained at 420 nm. The typical absorption spectrum of AgNPs is in the band of 350–450 nm [6].

Decolourization studies using the AgNPs

The decolourization of malachite green dye using the synthesized AgNPs was carried out according to the BBD, and the results obtained are given in Table 5.

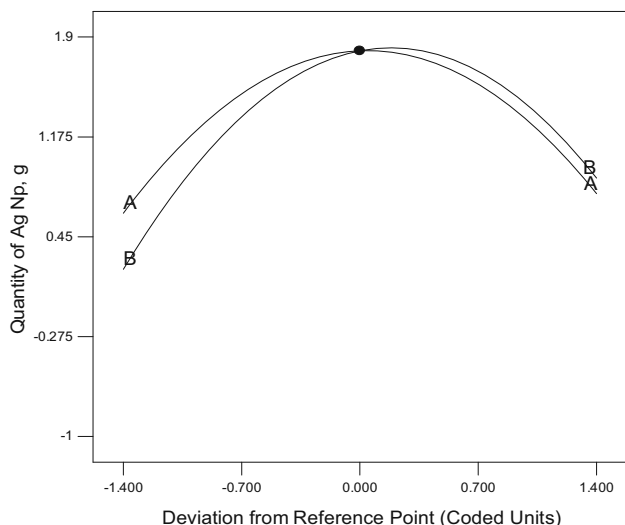


Fig. 2 Perturbation plot for AgNPs production

The mathematical expression of relationship to the response with variables is:

$$Y = 81.33 + 31.38A - 1.38B + 1.00C - 1.00AB + 0.75AC + 1.75BC - 37.67A^2 + 1.83B^2 + 2.58C^2 \quad (6)$$

where Y is the % removal of MG dye and A , B and C are the coded values of pH, temperature and AgNPs dosage.

The ANOVA results for decolourization of MG are tabulated in Table 6. F value of 146.97 implies that the model was significant. The Fisher F test with a very low probability value ($P_{\text{model}} > 0.0001$) reveals a very high significance for the regression model. The goodness of fit of the model was checked by coefficient of determination (R^2). The R^2 was found to be 0.9962, which implies that more than 99.62% of experimental data were compatible with the data predicted by the model. The deviations between experimental and predicted values were low, which was inferred from the CV value (4.99). The signal-to-noise ratio is given by Adeq precision. A ratio >4 is desirable. In the present work, the ratio was found to be 28.59, indicating an adequate signal. Value of " P " < 0.05

Fig. 3 UV-visible spectra for AgNPs

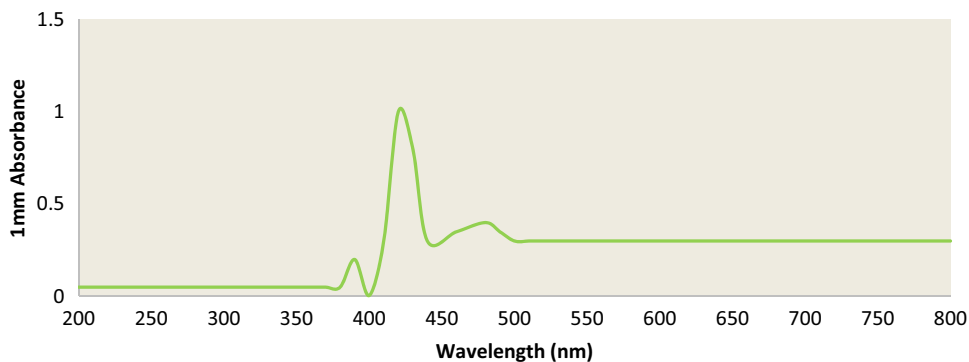


Table 5 BBD-based experimental design and its response for MG dye removal

Run order	A	B	C	% MG decolourization	
				Experimental	Predicted
1	-1	0	1	15	15.125
2	-1	1	0	16	13.750
3	-1	-1	0	14	14.500
4	1	-1	0	77	79.250
5	0	0	0	81	81.333
6	0	-1	1	87	86.375
7	1	0	-1	76	75.875
8	0	1	-1	81	81.625
9	1	1	0	75	74.500
10	0	1	1	85	87.125
11	0	0	0	85	81.333
12	-1	0	-1	13	14.625
13	1	0	1	81	79.375
14	0	-1	-1	90	87.875
15	0	0	0	78	81.333

indicates the significance of model terms. In this case, A and A^2 were significant model terms for the maximum decolourization of malachite green. This implies that the linear, square effects of pH were significant factors.

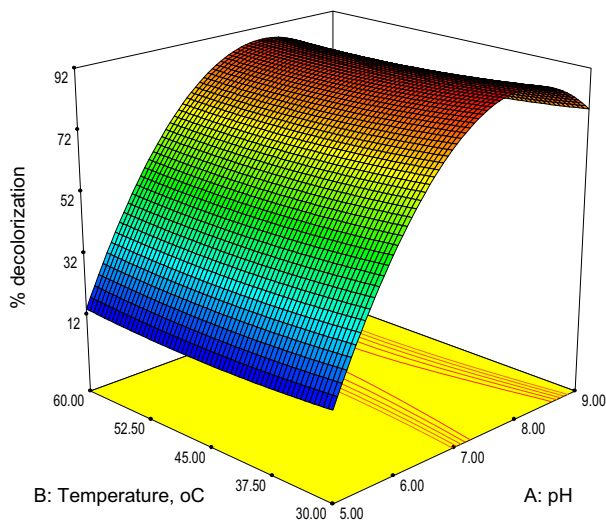
Effect of pH on decolourization

The effect of pH on decolourization of malachite green dye was studied by changing the pH from 5 to 9. The result obtained is shown in Figs. 4 and 6. From the plot, it can be inferred that in alkaline pH range of 7.5–9 higher percentage of decolourization was obtained and maximum percentage of decolourization was observed at a pH of 7.8. The percentage of decolourization was comparatively less in the acidic range. The dye adsorption is unfavourable at acidic pH values. This may be because (1) in acidic system, the number of negatively charged adsorbent sites decreased and the number of positively charged surface sites

Table 6 ANOVA for sorption of malachite green

Source	Sum of squares	df	Mean square	F value	P value
Model	13337.18	9	1481.91	146.97	<0.0001
A	7875.13	1	7875.13	781.00	<0.0001
B	15.13	1	15.13	1.50	0.2752
C	8.00	1	8.00	0.79	0.4139
AB	4.00	1	4.00	0.40	0.5565
AC	2.25	1	2.25	0.22	0.6566
BC	12.25	1	12.25	1.21	0.3206
A ²	5238.56	1	5238.56	519.53	<0.0001
B ²	12.41	1	12.41	1.23	0.3177
C ²	24.64	1	24.64	2.44	0.1788
Residual	50.42	5	10.08	0.70	0.6350
Lack of fit	25.75	3	8.58		
Pure error	24.67	2	12.33		
Cor total	133387.60	14			

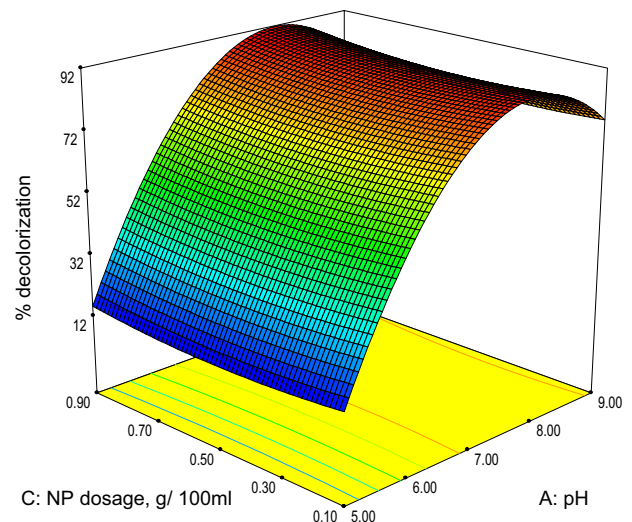
SD 0.318, R^2 0.9962, mean 63.60, adj. R^2 0.9895, CV% 4.99, pred. R^2 0.9651, PRESS 467.50, Adeq precision 28.590

**Fig. 4** Interactive effect of pH and temperature on MG decolourization using AgNPs

increased, which does not favour the adsorption of positively charged dye cations due to electrostatic repulsion and (2) lower adsorption of MG at acidic pH is due to the presence of excess H⁺ ions competing with dye cations for the adsorption sites of the adsorbent [20, 50].

Effect of temperature on decolourization

The effect of temperature on decolourization of malachite green dye was studied by changing the temperature from 30 to 60 °C. The result obtained is shown in Figs. 4 and 5. From the plot, it was inferred that the decolourization was favourable around 30–35 °C and 30 °C was found to be the optimum temperature for higher decolourization. An

**Fig. 5** Interactive effect of pH and AgNPs dosage on MG decolourization

increase in temperature decreases the specific uptake. This is probably caused by a change in the texture of the sorbent and a loss in the sorption capacity due to material deterioration [73]. Similar results were obtained by Abou-Gamra [1].

Effect of AgNPs dosage on decolourization

The effect of AgNPs dosage on decolourization of malachite green dye was studied by changing the AgNPs from 0.1 to 0.9 g/100 mL. The results obtained are shown in Figs. 5 and 6. It was inferred that the effect of dosage was dependent on interactive effects between pH and temperature. The dye uptake depends on the adsorption sites

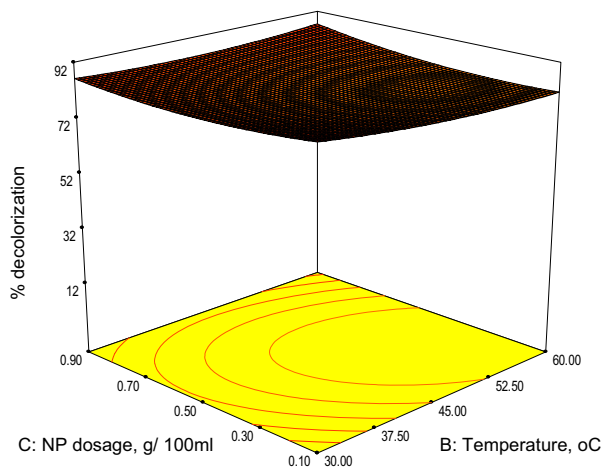


Fig. 6 Interactive effect of temperature and AgNPs dosage on MG decolorization

present in the sorbent [30]. As the sorbent dosage increases, the available adsorption site increases, facilitating higher percentage of dye removal. However, in the present study, at low dosage itself the maximum removal occurs. It shows that the sites required for the dye uptake are available at low dosage. The optimum quantity of AgNPs was found to be 0.1 g/100 mL, giving maximum decolourization of 90% at pH 7.8 and temperature 30 °C.

Equilibrium isotherm study

To study the mechanism of decolourization by sorption using AgNP, the batch experimental data were applied to the linear isotherms, namely Langmuir, Freundlich, Dubinin–Radushkevich, Temkin and three-parameter Sips isotherm.

Langmuir isotherm

A theory describing the sorption of gas molecules onto metal surfaces was proposed by Langmuir [39]. The Langmuir isotherm in linear form is given by:

$$\frac{1}{q_e} = \frac{1}{q_m b C_e} + \frac{1}{q_m} \tag{7}$$

where q_m is the monolayer sorption capacity of the sorbent (mg/g), q_e is the equilibrium dye concentration on the sorbent (mg/g), C_e is the equilibrium concentration of dye in the solution (mg/L), and b is the Langmuir sorption constant (l/mg) related to the free energy of sorption.

The Langmuir adsorption isotherm suggests monolayer coverage of adsorbed molecules [63, 64, 69]. The Langmuir plots of MG sorption isotherm with different initial dye concentrations are shown in Fig. 7. The constants q_m and b are tabulated in Table 7. The constant b denotes the

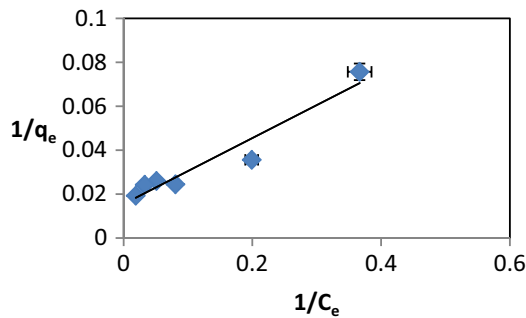


Fig. 7 Langmuir isotherm plot for the sorption of MG dye onto AgNPs

Table 7 Isotherm constants for the decolourization of malachite green by AgNPs

Isotherm model	Parameters	Values
Langmuir	q_{max}	64.5161 mg/g
	B	0.1033
	R^2	0.9292
Freundlich	K_f	11.7841
	$1/n$	0.3957
	R^2	0.8216
Dubinin–Radushkevich	q_{max}	43.8160 mg/g
	β	1.958
	ϵ	0.5053
	R^2	0.963
Temkin	B	11.34
	K_T	1.7338
	R^2	0.9030
Sips	a_s	6.006
	K_s	1.345
	β_s	0.1231
	R^2	0.9142

affinity between sorbent and sorbate. A high q_{max} and a high R^2 (0.9292) are the characteristics of good sorbent.

From the results, it was observed that the befitting nature of the above-mentioned isotherm model suggests that both homogeneous and heterogeneous sites are involved in accomplishing the process of adsorption. A probable chemical adsorption, through the ion exchange mechanism [75], is suggestive of the homogeneous monolayer distribution of the active sites, as indicated by the Langmuir isotherm.

Freundlich isotherm

The heterogeneous systems are represented by an empirical equation of the Freundlich isotherm [14], and the linear form of Freundlich isotherm is represented by the equation:

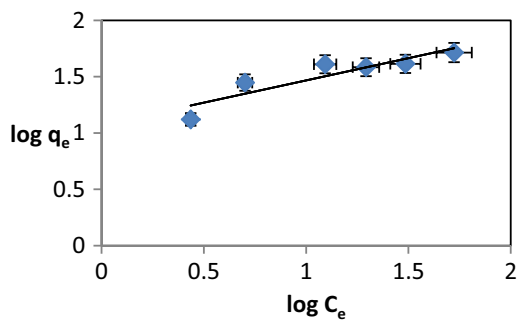


Fig. 8 Freundlich isotherm plot for the sorption of MG dye onto AgNPs

$$\log q_e = \log K_f + \frac{1}{n} \log C_e \tag{8}$$

where K_f is a constant relating the sorption capacity and $1/n$ is an empirical parameter relating the sorption intensity, which varies with the heterogeneity of the material. K_f value of 11.7841 and $1/n$ value of 0.3957 were obtained from the plot. Value of $1/n$ between 0 and 1 is the indication of good sorption [65–68]. In the present study, a value of 0.3957 was obtained and it indicates that the sorption of MG dye onto the AgNPs was favourable. Figure 8 shows the MG sorption isotherms at different initial dye concentrations of Freundlich, and the constants K_f and $1/n$ are tabulated in Table 7. From the plot of $\log q_e$ versus $\log C_e$, the slope value represents K_f and intercepts value represents $1/n$. In general, Freundlich isotherm predicts infinite surface coverage, indicating multilayer sorption on the surface, and does not predict any saturation of the adsorbent by the sorbate. The Freundlich constant ($1/n$) is estimated to be 0.3957, which reflects a surface heterogeneity of the adsorbent. A physical sorption is reflected by the heterogeneous nature [75]. However, the R^2 value of Freundlich isotherm is lower than that of Langmuir isotherm model. Hence, the Langmuir isotherm fits the experimental data better than the Freundlich isotherm.

Dubinin–Radushkevich isotherm

Equation 9 represents the linear form of the D–R isotherm equation [12]:

$$\ln q_e = \ln q_m - \beta \varepsilon^2 \tag{9}$$

where q_e is the amount of dye adsorbed per unit weight of sorbent (mg/g), q_m is the maximum sorption capacity (mg/g), β is the activity coefficient related to sorption mean energy (mol^2/kJ^2), and ε is the Polanyi potential described as

$$\varepsilon = RT \ln 1 + \frac{1}{C_e} \tag{10}$$

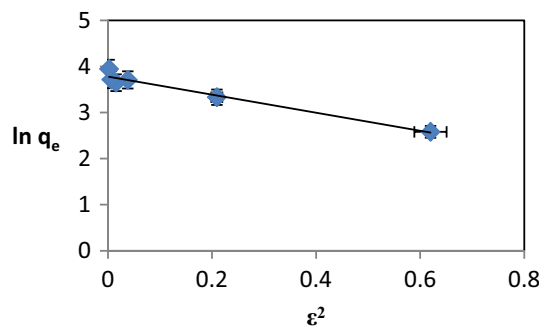


Fig. 9 Dubinin–Radushkevich isotherm plot for the sorption of MG dye onto AgNPs

where R is the gas constant 8.314×10^{-3} kJ/mol K, T is the temperature in K, and C_e is the equilibrium concentration of the MG dye in solution (mg/L). The mean free energy of sorption per molecule of sorbate required to transfer 1 mol of ion from the infinity in the solution to the surface of sorbent can be determined by Eq. (11):

$$E = \frac{1}{\sqrt{-2\beta}} \tag{11}$$

The slope and intercept value of the plot (Fig. 9) $\ln q_e$ versus ε give the Dubinin–Radushkevich constants β and q_m , and the results are tabulated in Table 7. The obtained energy value of $E < 8$ kJ/mol (Table 7) indicates that the adsorption is a physical process as chemical adsorption process has an $E > 8$ kJ/mol [24, 40]. A low sorption capacity compared to the Langmuir model can be attributed to different assumptions taken into consideration. Further based on the R^2 values, it was found that the Dubinin–Radushkevich isotherm model had a higher value compared to the other isotherm models. The supporting data that the Dubinin–Radushkevich isotherm model originally formulated for the adsorption process follow a pore-filling mechanism. It is generally applied to express the adsorption process occurred on both homogeneous and heterogeneous surfaces [7]. Moreover, it is reported that when the value of E is below 8 kJ/mol, the adsorption process can be considered as the physical adsorption. In contrast, if the value of E is located in the range of 8–16 kJ/mol, it is the chemical adsorption. From Table 7, it can be observed that the obtained values of mean free energy, E , is in the range of 0.5053 kJ/mol. Based on these data, it can thus be concluded that the effect of physical adsorption will play a dominating role in the adsorption process of malachite green dye adsorption onto the adsorbent [10, 52].

Temkin isotherm

The representation of Temkin isotherm [60] is as follows:

$$q_e = \frac{RT}{b} \ln K_T + \frac{RT}{b} \ln C_e \tag{12}$$

$$q_e = B \ln K_T + B \ln C_e \tag{13}$$

where constant $B = RT/b$, which is related to the heat of sorption, R is the universal gas constant (kJ/mol K), T is the temperature (K), b is the variation of sorption energy (J/mol), and K_T is the equilibrium binding constant (L/mg) corresponding to the maximum binding energy. From the plot, q_e versus $\ln C_e$ (Fig. 10), the constants B and K_T were found and are given in Table 7. Temkin isotherm model takes into account the adsorbent–adsorbate interactions on adsorption. It is based on the assumption that, due to the adsorbate–adsorbate repulsions, the heat of adsorption of all the molecules in the layer decreases linearly with the coverage of molecules and the adsorption of adsorbate is uniformly distributed. The constant B related to the heat of adsorption and K_T corresponds to the maximum binding energy. The correlation factors show that the Dubinin–Radushkevich model approximation to the experimental results was better than the Temkin model. Consequently, among the four isotherm models used, the Dubinin–Radushkevich model offers the best correlation factors.

Sips isotherm

A similar form to that of the Freundlich isotherm proposed by Sips in 1948 differs only on the finite limit of adsorbed amount at sufficiently high concentration.

$$q_e = \frac{K_s C_s^{\beta_s}}{1 + a_s C_e^{\beta_s}} \tag{14}$$

The parameter β_s is regarded as the parameter characterizing the system’s heterogeneity. The heterogeneity of the system comprises the sorbent or the dye, or a combination of both. All of the Sips parameters such as a_s , K_s and β_s were governed by operating conditions such as pH and temperature. The model is shown in Fig. 11, and the results are given in Table 7. In the adsorption of MG dye on AgNPs, the

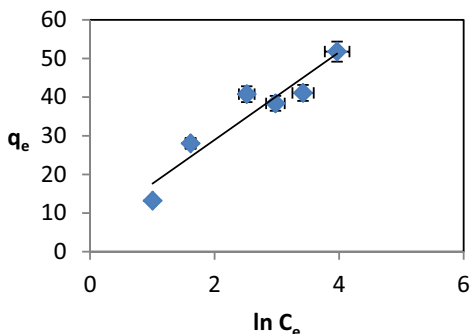


Fig. 10 Temkin isotherm plot for the sorption of MG dye onto AgNPs

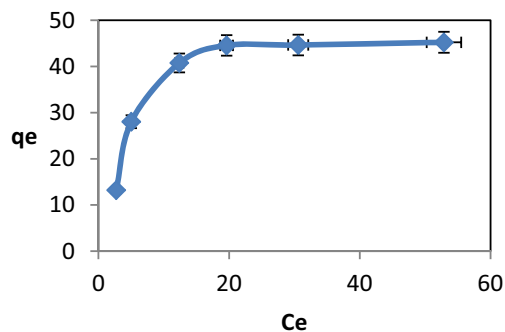


Fig. 11 Sips isotherm plot for the sorption of MG dye onto AgNPs at temperature 303.15 K

Table 8 Operation factor (K_R) values

Values of K_R	Condition of isotherm
$K_R > 1$	Unfavourable
$K_R = 1$	Linear
$0 < K_R < 1$	Favourable
$K_R = 0$	Irreversible

parameter β_s stays close to unity [3]. Sips isotherm model combines the Freundlich and Langmuir isotherms, thus convenient in studying the homogeneous and heterogeneous nature of the adsorption process. Constant β_s is often regarded as the heterogeneity factor, with values >1 indicating a heterogeneous system. Values close to (or exactly) 1 indicate a material with relatively homogenous binding sites. For $\beta_s = 1$, the Sips model reduces to the Langmuir equation. From Table 7, it was found that the value of β_s is 0.1231; thus, it indicates a homogeneous system. It was found that the correlation coefficient for Sips isotherm was low and hence the Dubinin–Radushkevich isotherm is considered to be more appropriate.

Separation factor to find the feasibility and condition of isotherm

The “favourable” or “unfavourable” conditions of an adsorption system can be predicted from effect of isotherm shape (Table 8) [49]. According to Hall et al. [19], the essential features of the Langmuir isotherm can be expressed in terms of a dimensionless constant separation factor or equilibrium parameter K_R , which is defined by the following relationship:

$$K_R = \frac{1}{1 + K_a C_0} \tag{15}$$

where K_R is a dimensionless separation factor, C_0 is initial dye concentration (mg/L), and K_a is isotherm constant (L/mg). From Table 9, it was found that all isotherms were favourable since $0 < K_R < 1$.

Table 9 Separation factor and their condition to find the feasibility and type of isotherm

Type of isotherm	K_R	Condition of isotherm
Langmuir	0.2791	Favourable
Freundlich	0.0918	Favourable
Dubinin–Radushkevich	0.00508	Favourable
Temkin	0.0008	Favourable
Sips	0.2452	Favourable

Comparison of sorption capacities of various sorbents

The sorption capacity of the sorbents used in the present work is compared with the other sorbents for the removal

malachite green dye. Table 10 shows the dye uptake capacity of various sorbents used for previous and present work. The equilibrium uptake (q_e) is estimated from the experimental data using Langmuir isotherm. The maximum uptake for malachite green dye is found to be 64.5161 mg/g for chemically synthesized AgNPs. From the results, it is found that chemically synthesized AgNPs can be used to effectively remove malachite green dye.

Sorption kinetics

Equilibrium analysis is important to evaluate the affinity and capacity of a sorbent. However, it is also important to assess how sorption rates vary with aqueous dye concentration and are affected by sorption capacity or by the

Table 10 Sorption capacities of various sorbents used for the removal of malachite green dye

Sorbent	Sorption capacity (mg/g)	Source
Carbon prepared from <i>Borassus</i> bark	20.70	[4]
Potato peel	32.39	[16]
Neem sawdust	4.35	[33]
Rice husk	19.83	[29]
Unsaturated polyester Ce(IV) phosphate	1.01	[31]
Orange peel	14.30	[2]
Sugarcane dust	4.88	[32]
Activated carbon	40.06	[57]
<i>Ricinus communis</i>	24.39	[41]
<i>R. communis</i> activated carbon	27.78	[53]
<i>Limonia acidissima</i>	34.56	[55]
Commercial activated carbon	8.27	[42]
Kapok hull activated carbon	30.16	[58]
Anondonta shell	11.3	[13]
<i>Loligo tulgaris</i>	39.8	[13]
Sepia	3.48	[13]
Rubber wood sawdust	36.45	[36]
<i>Annona squamora</i>	25.28	[54]
Activated carbon—laboratory grade	42.18	[42]
Leaves of <i>Solanum tuberosum</i>	33.33	[18]
Stem of <i>S. tuberosum</i>	27	[18]
Waste fruit residues	37.03	[47]
Dried cashew nut bark carbon	20.09	[48]
Tamarind fruit shell	1.95	[51]
Leaves of <i>Daucus carota</i>	52.6	[38]
Carbon from <i>Arundo donax</i> root	8.69	[76]
Chlorella-based biomass	18.4	[61]
Stem of <i>D. carota</i>	43.4	[38]
Cellulose powder	2.422	[56]
Rapeseed cake	17.89	[23]
TiO ₂ nanoparticles	11.72	[1]
<i>A. flavus</i> -mediated AgNPs	44.21	[46]
Chemically synthesized AgNPs	64.51	Present study

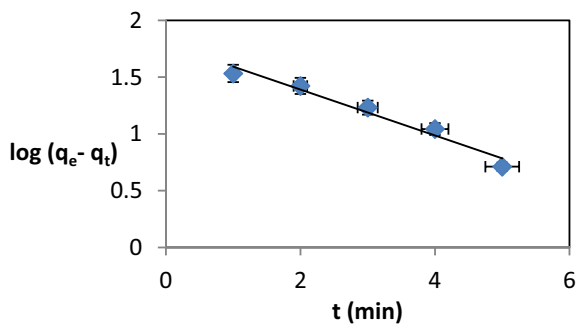


Fig. 12 Pseudo-first-order plot for sorption of MG dye onto AgNPs

sorbent character in terms of kinetics. The kinetic models such as pseudo-first-order, pseudo-second-order, intraparticle diffusion, power function and Elovich model were applied to interpret the experimental results.

Pseudo-first-order model

The pseudo-first-order equation for the sorption of a liquid–solid system based on the solid capacity was suggested by Lagergren [21]. The linear form of the pseudo-first-order rate equation is:

$$\log(q_e - q_t) = \log q_e - \frac{K_1}{2.303} t \tag{16}$$

where q_t and q_e (mg/g) are the amounts of the dye adsorbed at equilibrium (mg/g) and t (min), respectively, and K_1 is the rate constant of the equation (min^{-1}) [26, 27, 67, 68]. The sorption rate constant (K_1) is determined (Fig. 12), and the values are reported in Table 11.

Pseudo-second-order model

The sorption behaviour over the whole adsorption time is predicted by the pseudo-second-order model [22].

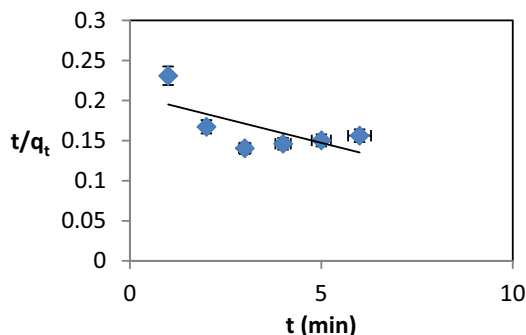


Fig. 13 Pseudo-second-order plot for sorption of MG dye onto AgNPs

$$\frac{t}{q_t} = \frac{1}{K_2 q_e^2} + \frac{1}{q_e} t \tag{17}$$

where K_2 (g/mg min) is the rate constant of the second-order equation and q_t (mg/g) is the amount of sorption equilibrium (mg/g) [26–28]. Sorption rate constants (K_2) are obtained experimentally by plot of t/q_t versus t (Fig. 13). The rate constants and R^2 values are given in Table 11. However, the correlation coefficients, R^2 , showed that the pseudo-first-order model fits better than the pseudo-second-order model.

Intraparticle diffusion model

Intraparticle diffusion model was given by Weber and Morris [74] and is represented by:

$$q_t = K_{id} t^{0.5} + C \tag{18}$$

where K_{id} is the intraparticle diffusion rate constant ($\text{mg/g min}^{0.5}$) and C is the intercept. It was inferred that all the plots have an initial curved portion, followed by a linear portion and a plateau region. The initial curve was due to the diffusion of dye through the solution to the external

Table 11 Kinetic parameters obtained from various kinetic models for sorption of MG

S. no.	Kinetic model	Parameters	MG sorption at temperature 303.15 K
1	Pseudo-first-order	K_1 (min^{-1})	0.4656
		R^2	0.9647
2	Pseudo-second-order	K_2 [(g/mg) min]	0.00006
		R^2	0.4465
3	Intraparticle diffusion	K_{id} [(g/mg) $\text{min}^{0.5}$]	23.981
		R^2	0.9964
4	Power function	K	6.5766
		V	0.6358
		R^2	0.9910
5	Elovich	α	20.7579
		β	0.0507
		R^2	0.9792

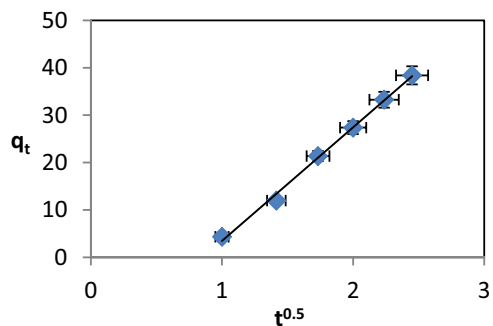


Fig. 14 Intraparticle diffusion plot for sorption of MG dye onto AgNPs

surface of AgNPs. The gradual sorption stage was described by the linear portion of curves, where intraparticle diffusion of dye on AgNPs takes place and equilibrium uptake is indicated by the final plateau region. Based on the results, it may be concluded that intraparticle diffusion is not only the rate-determining factor. The rate constants of intraparticle diffusion were calculated from Fig. 14. The values of constants for all the kinetic models were calculated and are summarized in Table 11. Higher values of R^2 show fitness of the sorption data [12, 40].

Power function model

The power function is given by

$$q = Kt^v \tag{19}$$

where q is amount of sorbate per unit mass of sorbent at time t , K and v are constants, and v is positive and <1 . Equation (19) is empirical, except for the case where $v = 0.5$, when it is similar to the parabolic diffusion equation, Eq. (19). Researchers have also used various modified forms for studying the kinetics of reactions on natural materials [37]. The constants of power function were calculated from Fig. 15 and are summarized in Table 11.

Elovich model

The Elovich equation (20) [44] incorporates α as the initial adsorption rate (mg/g min) and β (g/mg) as the desorption constant, thus relating the extent of the surface coverage and activation energy for chemisorptions.

$$\frac{dq}{dt} = \alpha e^{-\beta q} \tag{20}$$

Equation (20) can be simplified to Eq. (21) considering $\alpha\beta \gg t$ and by applying the boundary conditions $q_t = 0$ at $t = 0$ and $q_t = q_t$ at $t = t$

$$q_t = \frac{1}{\beta} \ln \alpha\beta + \frac{1}{\beta} \ln(t) \tag{21}$$

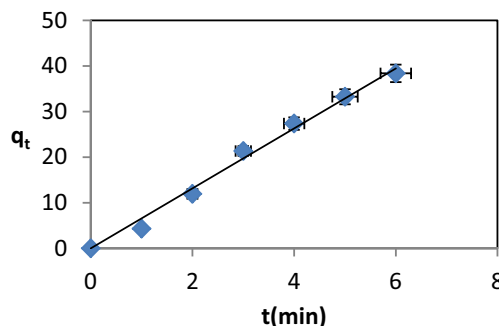


Fig. 15 Power function plot for sorption of MG dye onto AgNPs

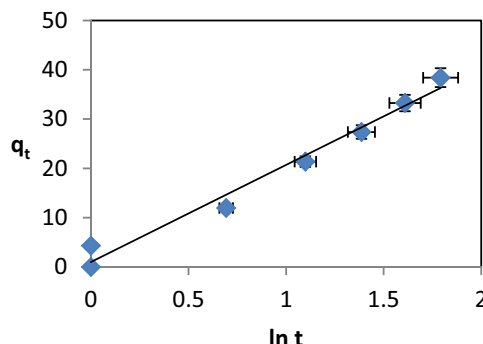


Fig. 16 Elovich diffusion plot for sorption of MG dye onto AgNPs

where q_t is the amount of gas chemisorbed at time t . From Table 11, it was found that the decolorization of MG fits the Elovich model [24]. A plot of q_t versus $\ln(t)$ (Fig. 16) with $(1/\beta)$ as slope and $(1/\beta)\ln(\alpha\beta)$ as intercept should give a linear relationship.

Discussion on kinetics model

From the kinetic parameters obtained (Table 11), it may be inferred that pseudo-first-order model has higher correlation coefficient compared to pseudo-second-order kinetic model; thus, pseudo-first-order model may be one of the routes for the adsorption of malachite green dye as suggested by the value of the correlation coefficients. Elovich equation is also used successfully to describe the second-order kinetics, assuming that the actual solid surfaces are energetically heterogeneous, but the equation does not propose any definite mechanism for adsorbate–adsorbent interactions. The power function model is a modified form of the Freundlich equation. Figure 15 shows that, although a linear relationship existed over the sorption process, based on the higher correlation coefficient value of the intraparticle diffusion, it is inferred that intraparticle diffusion plays a significant role in the adsorption of malachite green dye. The intraparticle diffusion mechanism is as follows: there are essentially three consecutive mass

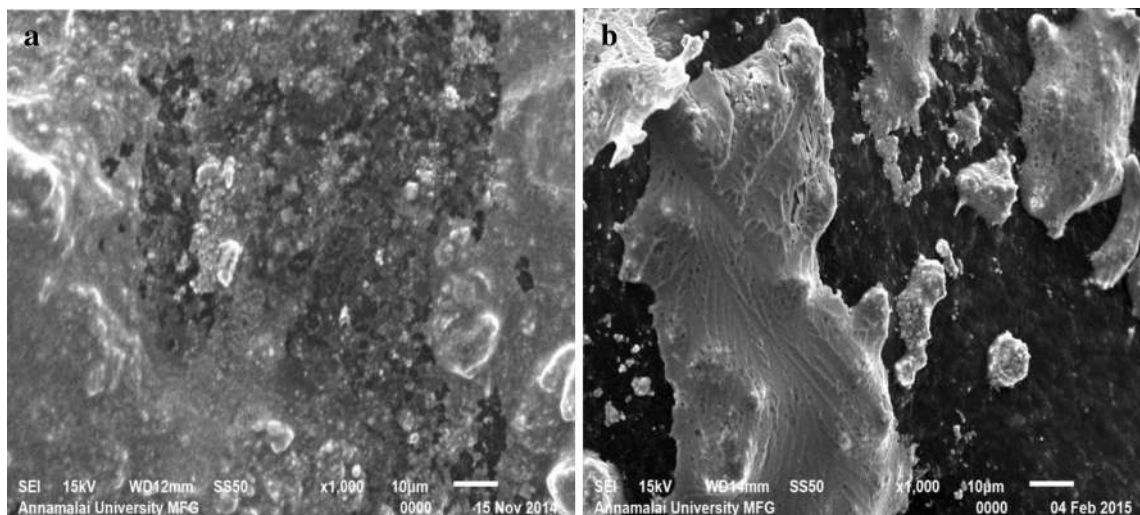


Fig. 17 **a** AgNPs before sorption, **b** AgNPs after sorption

transport steps associated with the adsorption of solute from the solution by an adsorbent. These are (1) film diffusion, (2) intraparticle or pore diffusion, and (3) sorption into interior sites. The third step is very rapid, and hence, film and pore transports are the major steps controlling the rate of adsorption. The value of intercept gives an idea about the thickness of boundary layer, i.e. the larger the intercept, the greater the boundary layer. Since the linear portion (Fig. 14) does not pass through the origin, therefore it is not the rate-limiting step [8].

Scanning electron microscopy

SEM images were used for the study of morphological changes of AgNPs before and after treatment. The AgNPs before treatment were individual and can be easily identified before the treatment (size ranges from 100 to 500 nm approx.). After the sorption process, they intend to agglomerate, which can be observed from Fig. 17b. It confirms that the sorption of MG dye took place efficiently. The surface which was rough prior to sorption has become smooth after the sorption.

Fourier transform infrared spectroscopy (FTIR) analysis

The FTIR spectrum of the sorbent before and after sorption analysed in the region $4000\text{--}400\text{ cm}^{-1}$ is shown in Fig. 18a, b. The binding of dyes to sorbents is mainly due to many chemical functional groups, namely hydroxyl, carboxyl, amine, sulphonic and ester groups, and they are identified as potential adsorption sites. The wide band at 3450.55 cm^{-1} shown in the spectrum of sorbent is attributed to stretching vibration of hydroxyl group of sorbents.

The band at 2922.23 cm^{-1} shown in the spectrum is assigned to the C–H stretching vibration of polymer backbone. The band at 1384 cm^{-1} in the spectrum is assigned to a symmetrical deformation of the CH_3 group. The bands observed at 1628 cm^{-1} correspond to N–H bonding vibrations. The band at $23,851\text{ cm}^{-1}$ has a larger intensity, which suggests effective deacetylation. In the spectrum, the presence of bands, at 1020 cm^{-1} , probably indicates the stretching vibrations of C–O group. After adsorption, there is no change in first band and a small change is observed in the second band, which indicates that no significant interaction occurs between C and O groups of AgNPs and dye. The shifting of peaks after adsorption of dye onto chemically synthesized AgNPs is shown in Table 12. Significant changes were observed in the peak values, which indicate the existence of physical interaction between dye and the AgNPs. Dolphen and Thiravetyan [11] have reported similar shifting phenomenon with the adsorption and have also stated that the shifting was due to electrostatic and chemical adsorption. This shift in peak values may be due to the formation of chemical bond between functional groups present on AgNPs and MG [55]. Similar shifting was recorded by Tang et al. [59] for adsorption of malachite green dye.

Mechanism of adsorption

According to Gulipalli et al. [17], the process of adsorption occurs either in single step or in combination of the steps such as film or external diffusion, pore diffusion, surface diffusion and adsorption on the pore surface. It was also reported that adsorption of on the adsorbent surface proceeds in three steps: (1) migration to the surface, (2) dissociation (or deprotonation) of complexes in aqueous

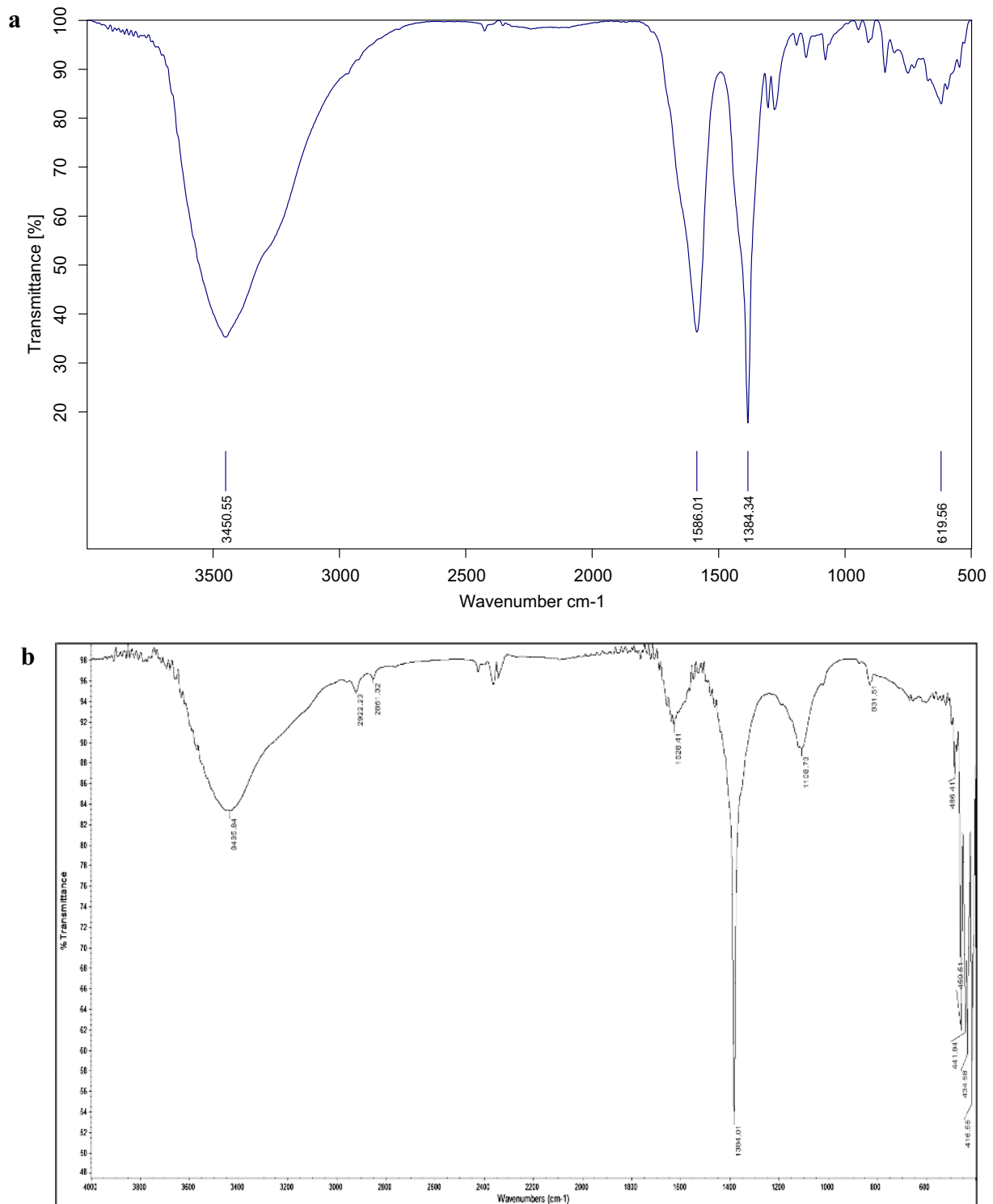


Fig. 18 **a** FTIR spectra of AgNPs before sorption, **b** FTIR spectra of AgNPs after sorption

solution, and (3) surface complexation [35, 77]. Adsorbate is diffused on external surface of the adsorbent (nanoadsorbents) due to diffusion potential characterized by the concentrations of adsorbate and available external surface area on the adsorbent. After diffusion on the external surface of

the adsorbent, adsorbate is diffused on the available pores of the adsorbent. All the available exposed active sites are occupied during the adsorption process governed by either physisorption or chemisorption.

Table 12 FTIR spectral characteristics of AgNPs before and after sorption of MG dye

Wavelength range (cm ⁻¹)	AgNP			Assignment
	Before loading of dye	After loading of dye	Differences	
3500–3000	3450.50	3435.84	–14.66	Bonded –OH groups
2900–2800	–	2922.23	+2922.23	CH stretching
	–	2851.32	+2851.32	
1740–1680	1686.11	1628.41	–57.05	C=O carbonyl groups
1500–1300	1384.34	1384.01	–0.33	C–O stretch
1150–850	–	1108.73	+1108.73	–PO ₄ ³⁻ stretching
	–	831.51	+831.51	
650–480		486.41	+486.41	N-containing bioligands
		450.61	+450.61	
		441.94	+441.94	
		434.58	+434.58	
		416.55	+416.55	

Conclusions

In this study, the sorption of malachite green onto chemically synthesized AgNPs was studied. RSM was utilized to optimize the production maximization of AgNPs and also for the sorption of malachite green. Maximum of 1.8 g/100 mL of AgNPs was obtained. Analysis of variance showed a high coefficient of determination value for enhanced production and sorption of malachite green ensuring a satisfactory adjustment of the second-order regression model with the experimental data. Sorption kinetics followed intraparticle diffusion and power function model. Experimental data were analysed using Langmuir, Freundlich, Dubinin–Radushkevich, Temkin and Sips isotherm models, and it was found that the Dubinin–Radushkevich presented a better fit. The findings of the present study indicated that the chemically synthesized AgNPs can be successfully used for the removal of malachite green dye.

References

- Abou-Gamra ZM, Ahmed MA (2015) TiO₂ nanoparticles for removal of malachite green dye from waste water. *Adv Chem Eng Sci* 5:373–388
- Annadurai G, Juang RS, Lee DJ (2002) Use of cellulose based wastes for adsorption of dyes from aqueous solutions. *J Hazard Mater B92*:263–274
- Apiratikul R, Pavasant P (2008) Batch and column studies of biosorption of heavy metals by *Caulerpa lentillifera*. *Bioresour Technol* 99:2766–2777
- Arivoli S, Hema M, Martin P, Prasath D (2009) Adsorption of malachite green onto carbon prepared from borassus bark. *Arab J Sci Eng* 34(2):31–42
- Arora S (2014) Textile dyes its impact on environment and treatment. *J Bioremediat Biodegener* 5(3):1
- Aslan K, Lakowicz JR, Geddes CD (2005) Rapid deposition of triangular silver nanoplates on planar surfaces: application to metal enhanced fluorescence. *J Phys Chem* 109(13):6247–6251
- Chen X (2015) Modeling of experimental adsorption isotherm data. *Information* 6:14–22
- Crank J (1965) *The mathematics of diffusion*. Clarendon Press, London
- Culp SJ, Beland FA, Heflich RH (2002) Mutagenicity and carcinogenicity in relation to DNA adduct formation in rats fed leucomalachite green. *Mutat Res* 506–507:55–63
- Dada AO, Olalekan AP, Olatunya AM, Dada O (2012) Langmuir, Freundlich, Temkin and Dubinin–Radushkevich isotherms studies of equilibrium sorption of Zn²⁺ unto phosphoric acid modified rice husk. *J Appl Chem* 3:38–45
- Dolphen R, Thiravetyan T (2011) Adsorption of melanoidins by chitin nanofibers. *Chem Eng J* 166:890–895
- Dubinin MM (1960) The potential theory of adsorption of gases and vapors for adsorbents with energetically nonuniform surfaces. *Chem Rev* 60:235–266
- Figueiredo SA, Boaventura RA, Loureiro JM (2000) Color removal with natural adsorbents: modeling, simulation and experimental. *Sep Purif Technol* 20:129–141
- Freundlich HMF (1906) Over the adsorption in solution. *J Phys Chem* 57:385–470
- Gessner T, Mayer U (2002) *Triarylmethane and diarylmethane dyes in Ullmann's encyclopedia of industrial chemistry*. Wiley-VCH, Weinheim
- Guechi EK, Hamdaoui O (2011) Sorption of malachite green from aqueous solution by potato peel: kinetics and equilibrium modeling using non-linear analysis method. *Arab J Chem*. doi:10.1016/j.arabjc.2011.05.011
- Gulipalli CS, Prasad B, Wasewar KL (2011) Batch study, equilibrium and kinetics of adsorption of selenium using rice husk ash (RHA). *J Eng Sci Technol* 6(5):586–605
- Gupta N, Kushwaha AK, Chatopadhyaya MC (2011) Application of potato (*Solanum tuberosum*) plant wastes for the removal of methylene blue and malachite green dye from aqueous solution. *Arab J Chem* 9:709–716

19. Hall KR, Eagleton LC, Acrivos A, Vermeulen T (1966) Pore and solid diffusion kinetics in fixed bed adsorption under constant-pattern conditions. *Ind Eng Chem Fundam* 5(2):212–223
20. Hamdaoui O (2006) Batch study of liquid-phase adsorption of methylene blue using cedar sawdust and crushed brick. *J Hazard Mater* 135(1):264–273
21. Ho YS (2004) Citation review of Lagergren kinetic rate equation on adsorption reactions. *Scientometrics* 59(1):171–177
22. Ho YS, McKay G (1999) Pseudo-second order model for sorption processes. *Process Biochem* 34:451–465
23. Jasinska A, Bernat P, Paraszkiwicz K (2013) Malachite green removal from aqueous solution using the system rapeseed press cake and fungus *Myrothecium roridum*. *Desalin Water Treat* 51(40–42):7663–7671
24. Javadian H, Ahmadi M, Ghiasvand M, Kahrizi S, Katal R (2013) Removal of Cr(VI) by modified brown algae *Sargassum bevanom* from aqueous solution and industrial wastewater. *J Taiwan Inst Chem E* 44:977–989
25. Junejo Y, Sirajuddin A, Baykal M, Safdar BA (2014) A novel green synthesis and characterization of AgNPs with its ultra rapid catalytic reduction of methyl green dye. *J Appl sci surf* 290:499–503
26. Kamaraj R, Vasudevan S (2016) Facile one-pot synthesis of nano-zinc hydroxide by electro-dissolution of zinc as a sacrificial anode and the application for adsorption of Th^{4+} , U^{4+} , and Ce^{4+} from aqueous solution. *Res Chem Intermed* 42:4077–4095
27. Kamaraj R, Vasudevan S (2016) Facile one pot electro synthesis of $\text{Al}(\text{OH})_3$ kinetics and equilibrium modeling for adsorption of 2,4,5-trichlorophenoxyacetic acid from aqueous solution. *New J Chem* 40:2249–2258
28. Kamaraj R, Pandiarajan A, Jayakiruba S, Naushad M, Vasudevan S (2016) Kinetics, thermodynamics and isotherm modeling for removal of nitrate from liquids by facile one-pot electrosynthesized nano zinc hydroxide. *J Mol Liq* 215:204–211
29. Kannan N, Sundaram MM (2001) Kinetics and mechanism of removal of methylene blue by adsorption of various carbons, a comparative study. *Dyes Pigment* 51:25–40
30. Karimi H, Mousavi S, Sadeghian B (2012) Silver nanoparticle loaded on activated carbon as efficient adsorbent for removal of methyl orange. *Indian J Sci Technol* 5:2346–2353
31. Khan AA, Ahmad R, Khan A, Mondal PK (2010) Preparation of unsaturated polyester Ce(IV) phosphate by plastic waste bottles and its application for removal of malachite green dye from water samples. *Arab J Chem*. doi:10.1016/j.arabjc.2010.10.012
32. Khattri SD, Singh MK (2000) Colour removal from synthetic dye wastewater using a biosorbent. *Water Air Soil Pollut* 120:283–294
33. Khattri SD, Singh MK (2009) Removal of malachite green from dye wastewater using neem sawdust by adsorption. *J Hazard Mater* 167:1089–1094
34. Kim KD, Han DN, Kim HT (2004) Optimization of experimental conditions based on the Taguchi robust design for the formation of nanosized silver nanoparticles by chemical reduction method. *J chem Eng* 104(1–3):55–61
35. Kong S, Wang Y, Zhan H, Yuan S, Yu M, Liu M (2014) Adsorption oxidation of arsenic in groundwater by nanoscale Fe–Mn binary oxides loaded on zeolite. *Water Environ Res* 86(2):147–155
36. Kumar KV, Sivanesan S (2007) Isotherms for malachite green onto rubber wood (*Hevea brasiliensis*) sawdust: comparison of linear and non-linear methods. *Dyes Pigment* 72(1):124–129
37. Kuo S, Lotse EG (1974) Kinetics of phosphate adsorption and desorption by lake sediments. *Soil Sci Soc Am J* 38:50–54
38. Kushwaha AK, Gupta N, Chattopadhyaya MC (2014) Removal of cationic methylene blue and malachite green dyes from aqueous solution by waste materials of *Daucus carota*. *Arab J Chem* 18:200–207
39. Langmuir I (1916) The adsorption of gases on plane surface of glass, mica and platinum. *J Am Chem Soc* 40:1361–1368
40. Lodeiro P, Barriada JL, Herrero de Vicente R, Sastre ME (2006) The marine microalga *Cystoseira baccata* as biosorbent for cadmium(II) and lead(II) removal: kinetic and equilibrium studies. *Environ Pollut* 142:264–273
41. Makeswari M, Santi T (2013) Removal of malachite green dye from aqueous solutions onto microwave assisted zinc chloride chemical activated Epicarp of *Ricinus communis*. *J Water Resour Prot* 5:222–238
42. Mall ID, Srivastava VC, Agarwal NK, Mishra IM (2005) Adsorptive removal of malachite green dye from aqueous solution by bagasse fly ash and activated carbon—kinetic study and equilibrium isotherm analyses. *Colloids Surf A* 264(1–3):17–28
43. Mie G (1908) Contributions to the optics of turbid media especially colloidal metal solutions. *Ann Phys* 25:377–445
44. Onal Y (2006) Kinetics of adsorption of dyes from aqueous solutions using apricot. *J Hazard Mater B* 137:1719–1728
45. Pandian AMK, Karthikeyan C, Rajasimman M, Dinesh MG (2015) Synthesis of silver nanoparticle and its application. *Ecotoxicol Environ Saf* 121:211–217
46. Pandian AMK, Karthikeyan C, Rajasimman M (2016) Isotherm and kinetic studies on nano-sorption of malachite green onto *Aspergillus flavus* mediated synthesis of silver nano particles. *Environ Nanotechnol Monit Manag* 6:139–151
47. Parimaladevi P, Venkateswaran V (2011) Kinetics, thermodynamics and isotherm modeling of adsorption of triphenylmethane dyes (methyl violet, malachite green and magenta II) on to fruit waste. *J Appl Technol Environ Sanit* 1(3):273–283
48. Parthasarathy S, Manju N, Hema M, Arivoli S (2011) Removal of malachite green from industrial wastewater by activated carbon prepared from cashew nut bark *Alfa universal*. *Int J Chem* 2(2):41–51
49. Poots VJP, McKay G, Healy JJ (1978) Removal of basic dye from effluent using wood as an adsorbent. *J Water Pollut Control Fed* 50:926–935
50. Rajeshkannan R, Rajasimman M, Rajamohan N (2010) Removal of malachite green from aqueous solution using *Hydrilla verticillata*—optimization, equilibrium and kinetic studies. *Int J Environ Chem Ecol Geol Geophys Eng* 4(1):23–30
51. Saha P, Chowdhury S, Gupta S, Kumar I, Kumar R (2010) Assessment on the removal of malachite green using tamarind fruit shell as biosorbent. *Clean Soil Air Water* 38(5–6):437–447
52. Samarghandi MR, Hadi M, Moayedi S, Askari FB (2009) Two-parameter isotherms of methyl orange sorption by pinecone derived activated carbon. *J Environ Health Sci Eng* 6:285–294
53. Santhi T, Manonmani S, Smitha T (2010) Removal of malachite green from aqueous solution by activated carbon prepared from the epicarp of *Ricinus communis* by adsorption. *J Hazard Mater* 179(1–3):178–186
54. Santhi T, Manonmani S, Smith T (2010) Removal of malachite green from aqueous solution by activated carbon prepared from the *Annona squamosa* seed by adsorption. *Electr J Chem* 2(2):101–117
55. Sartape AS, Mandhare AM, Jadhav VV, Raut PD, Anuse MA, Kolekar SS (2013) Removal of malachite green dye from aqueous solution with adsorption technique using *Limonia acidissima* (wood apple) shell as low cost adsorbent. *Arab J Chem*. doi:10.1016/j.arabjc.2013.12.019
56. Sekhar CP, Kalidhasan S, Rajesh V, Rajesh N (2009) Biopolymer adsorbent for the removal of malachite green from aqueous solution. *Chemosphere* 77(6):842–847
57. Sharma YC, Uma SV, Srivastava J, Mahato M (2007) Reclamation of Cr(VI) rich water and wastewater by wollastonite. *Chem Eng J* 127:151–156

58. Syed SPS (2011) Study of the removal of malachite green from aqueous solution by using solid agricultural waste. *Res J Chem Sci* 1(1):88–104
59. Tang H, Zhou W, Zhang L (2012) Adsorption isotherms and kinetics studies of malachite green on chitin hydrogels. *J Hazard Mater* 209–210:218–225
60. Temkin MJ, Pyzhev V (1940) Kinetics of ammonia synthesis on promoted iron catalysts. *Acta Physicochim URSS* 12:217–256
61. Tsai WT, Chen HR (2010) Removal of malachite green from aqueous solution using low-cost chlorella based biomass. *J Hazard Mater* 175:844–854
62. Vanaja M, Paulkumar K, Baburaja M, RajeshKumar S, Gnanajobitha G, Malarkodi C et al (2014) Degradation of methylene blue using biologically synthesized silver nanoparticles. *J Bioinorg Chem Appl* 1:1–7
63. Vasudevan S, Lakshmi J (2012) Process conditions and kinetics for the removal of copper from water by electrocoagulation. *Environ Eng Sci* 29:563–572
64. Vasudevan S, Lakshmi J (2012) Electrochemical removal of boron from water: adsorption and thermodynamic studies. *Can J Chem Eng* 90:1017–1026
65. Vasudevan S, Lakshmi J, Sozhan G (2009) Optimization of the process parameters for the removal of phosphate from drinking water by electrocoagulation. *Desalin Water Treat* 12:407–414
66. Vasudevan S, Jayaraj J, Lakshmi J, Sozhan G (2009) Removal of iron from drinking water by electrocoagulation: adsorption and kinetics studies. *Korean J Chem Eng* 26:1058–1064
67. Vasudevan S, Lakshmi J, Vanathi R (2010) Electrochemical coagulation for chromium removal: process optimization, kinetics, isotherms and sludge characterization. *Clean Soil Air Water* 38:9–16
68. Vasudevan S, Lakshmi J, Sozhan G (2010) Studies relating to removal of arsenate by electrochemical coagulation: optimization, kinetics, coagulant characterization. *Sep Sci Technol* 45:1313–1325
69. Vasudevan S, Lakshmi J, Kamaraj R, Sozhan G (2012) A critical study on the removal of copper by an electrochemically assisted coagulation: equilibrium, kinetics, and thermodynamics. *Asia Pac J Chem Eng* 8:162–171
70. Veterinary Residues Committee (2001) Annual report on surveillance for veterinary residues in residues in food in the UK. The Veterinary Residues Committee, Woodham Lane, New Haw, Addlestone, Surrey
71. Veterinary Residues Committee (2002) Annual report on surveillance for veterinary residues in residues in food in the UK. The Veterinary Residues Committee, Woodham Lane, New Haw, Addlestone, Surrey
72. Veterinary Residues Committee (2003) Annual report on surveillance for veterinary residues in residues in food in the UK. The Veterinary Residues Committee, Woodham Lane, New Haw, Addlestone, Surrey
73. Volesky B (2003) Sorption and biosorption. BV-Sorbex, Montreal
74. Weber WJ, Morris JC (1963) Kinetics of adsorption on carbon from solution. *J Sanit Eng Div Am Soc Civil Eng* 89:31–60
75. Yasemin B, Zeki T (2007) Removal of heavy metals from aqueous solution by sawdust adsorption. *J Environ Sci* 19:160–166
76. Zhang J, Li Y, Zhang C, Jing Y (2008) Adsorption of malachite green from aqueous solution onto carbon prepared from *Arundo donax* root. *J Hazard Mater* 50:774–782
77. Zhu H, Jia Y, Wua X, Wanga H (2009) Removal of arsenic from water by supported nano zero-valent iron on activated carbon. *J Hazard Mater* 172:1591–1596